

Aragonite and Unusual Pigments Identification

Subjects: Art | Chemistry, Analytical | Spectroscopy

Contributor: Laura Rampazzi

Aragonite is a mineralogical form of calcium carbonate, mainly of biogenic origin. Historical sources report its use in Roman times as an aggregate in mortars, and in the literature it has only been shown in Roman wall paintings. Thus, its use in 16th century wall paintings of the church of Santo Stefano in Selva (Cerignale, Apennines of central Italy) is surprising.

Keywords: aragonite ; Brunswick green ; clinocllore

1. Introduction

The church of Santo Stefano in Selva (Cerignale) (**Figure 1**), in the Apennines of Piacenza (central Italy), is in a declining state of neglect and decay. Given its location in a remote area, with no tourism, it is not a high priority for the national heritage. The local community pressed for an analytical campaign on the fragments of the few surviving paintings, in order to preserve their memory.



Figure 1. The remains of wall paintings in the church of S. Stefano.

The area between the Po Valley and the Ligurian Sea was once much travelled, and there were also several historical pilgrimages, along important trade ridgeways, such as the salt routes, which involved the exchange of local goods. One of these routes, the “Strada del Cifalco”, followed the natural path of the Trebbia Valley along the ridge between the Aveto and Trebbia rivers, connecting the north of what today is Liguria with Piacenza. It is thus not surprising that the Apennines, the mountainous system of this area, are rich in artistic testimonies, which unfortunately were neglected during the depopulation after the Second World War. This artistic history can be seen in the municipality of Cerignale too: the village of Ponte Organasco, with its medieval layout and many tower houses; the medieval castle of Cariseto, which hosted Emperor Frederick Barbarossa; and the church of Santo Stefano in Selva. The building is located in an area which was once a point of transit and rest for the muleteers travelling between the Trebbia valley and the Aveto valley, on their way to Liguria.

Documentation on the history of the paintings is scarce. The building is listed in a church register which records the

churches that in 1523 sent financial dues to the Papal State. The ruins still reveal the elaborate construction technique adopted to simulate a certain opulence, such as the vaulted ceiling, which looks like it is made of stone, but is actually a wooden structure with the intrados made of reeds covered with painted plaster. The facade of the single-nave church is relatively intact, and recalls the classical Greek temple structure. The lesenes support the very elaborate trabeation and triangular tympanum. Three transverse round arches have also remained intact. No records of the wall paintings have been found in the archives. We can thus only assume that the first cycle of paintings dates back to the construction of the building in the 16th century.

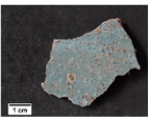
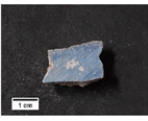
The church has almost completely lost the internal wall paintings (**Figure 1**). The decay originated from the partial settlement of the ground, around the middle of the last century, and more recently from a bolt of lightning that hit the stone bell tower causing a fire that almost completely destroyed the roof.

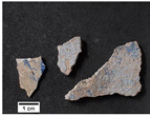
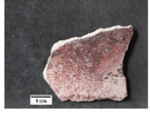
The present work reports the analytical campaign conducted on fragments from the few wall paintings still in place. The samples were analyzed with optical microscopy and scanning electron microscopy equipped with an energy-dispersive spectrometer, also on polished cross sections, and with X-ray diffraction and infrared spectroscopy on powders. The analyses obtained important information on the pictorial materials, pigments and binders used for the decoration of the walls. Traditional and unusual pigments were revealed together with the widespread use of aragonite probably from shells utilized as a building material.

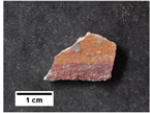
2. Research

The fragments analyzed had different colored layers that were identified by IR spectra and XRD analysis of the powders or suggested by EDX elemental spectra and maps (**Table 1**).

Table 1. Description of the samples, identified pigments and employed analytical techniques (OM: optical microscopy; FTIR-ATR: Fourier-transform infrared spectroscopy in attenuated total reflection; XRD: X-ray diffraction; SEM-EDX: scanning electron microscopy-energy dispersive X-ray spectroscopy; PCS: polished cross section).

Sample	Images	Colors	Identified Pigments	Analytical Techniques
ST1		aqua green	blanc fixe (BaSO ₄), clinocllore (Mg ₄ Fe ₂ Al(Si ₃ Al)O ₁₀ (OH) ₈), ultramarine blue (Na ₈ Al ₆ Si ₆ O ₂₄ S ₄)	OM, FTIR-ATR, XRD, SEM-EDX
ST2		aqua green	blanc fixe (BaSO ₄), ultramarine blue (Na ₈ Al ₆ Si ₆ O ₂₄ S ₄)	FTIR-ATR, XRD, SEM-EDX, PCS
		blue	ultramarine blue (Na ₈ Al ₆ Si ₆ O ₂₄ S ₄)	
		red	red ochre (Fe ₂ O ₃ , clay)	
		white	blanc fixe (BaSO ₄)	
		white	bianco di Sangiovanni (CaCO ₃)	
ST3		aqua green	ultramarine blue (Na ₈ Al ₆ Si ₆ O ₂₄ S ₄), ultramarine yellow (BaCrO ₄)	FTIR-ATR, SEM-EDX, PCS
		blue	ultramarine blue (Na ₈ Al ₆ Si ₆ O ₂₄ S ₄)	
		white	bianco di Sangiovanni (CaCO ₃)	
		yellow	yellow ochre (FeOOH, clay)	
ST4		blue	ultramarine blue (Na ₈ Al ₆ Si ₆ O ₂₄ S ₄)	FTIR-ATR, XRD, SEM-EDX
ST5		blue	ultramarine blue (Na ₈ Al ₆ Si ₆ O ₂₄ S ₄)	OM, FTIR-ATR, XRD, SEM-EDX, PCS
		red	red ochre (Fe ₂ O ₃ , clay)	
		white	bianco di Sangiovanni (CaCO ₃)	

Sample	Images	Colors	Identified Pigments	Analytical Techniques
ST6		blue	ultramarine blue ($\text{Na}_8\text{Al}_6\text{Si}_6\text{O}_{24}\text{S}_4$)	FTIR-ATR, XRD, SEM-EDX
		red	red ochre (Fe_2O_3 , clay)	
		yellow	cinnabar/vermilion (HgS), yellow ochre (FeOOH , clay)	
ST7		black	red ochre (Fe_2O_3 , clay)	OM, FTIR-ATR, SEM-EDX
		blue	blanc fixe (BaSO_4), ultramarine blue ($\text{Na}_8\text{Al}_6\text{Si}_6\text{O}_{24}\text{S}_4$)	
		light blue	blanc fixe (BaSO_4), ultramarine blue ($\text{Na}_8\text{Al}_6\text{Si}_6\text{O}_{24}\text{S}_4$), white lead ($2\text{PbCO}_3 \cdot \text{Pb}(\text{OH})_2$)	
		grey	manganese black (MnO_2), yellow ochre (FeOOH , clay)	
		dark ochre	manganese black (MnO_2), yellow ochre (FeOOH , clay)	
		yellow	yellow ochre (FeOOH , clay)	
ST8		green	Brunswick green ($(\text{Cu,Zn})_2(\text{OH})_3\text{Cl}$)	OM, FTIR-ATR, XRD, SEM-EDX
		orange	yellow ochre (FeOOH , clay)	
		yellow	chrome yellow (PbCrO_4)	
ST9		ochre	yellow ochre (FeOOH , clay)	FTIR-ATR, SEM-EDX
ST10		red	red ochre (Fe_2O_3 , clay)	OM, FTIR-ATR, SEM-EDX
		yellow	yellow ochre (FeOOH , clay)	
ST11		green	Brunswick green ($(\text{Cu,Zn})_2(\text{OH})_3\text{Cl}$)	OM, FTIR-ATR, XRD, SEM-EDX
		yellow	chrome yellow (PbCrO_4), yellow ochre (FeOOH , clay)	
ST12		red	cinnabar/vermilion (HgS)	FTIR-ATR, SEM-EDX
		yellow	chrome yellow (PbCrO_4), yellow ochre (FeOOH , clay)	
ST13		red	cinnabar/vermilion (HgS), yellow ochre (FeOOH , clay)	FTIR-ATR, SEM-EDX
		yellow	chrome yellow (PbCrO_4), ultramarine yellow (BaCrO_4)	
ST14		blue	ultramarine blue ($\text{Na}_8\text{Al}_6\text{Si}_6\text{O}_{24}\text{S}_4$)	FTIR-ATR, SEM-EDX, PCS
		red	cinnabar/vermilion (HgS), red ochre (Fe_2O_3 , clay)	
		white	bianco di Sangiovanni (CaCO_3)	
		yellow	chrome yellow (PbCrO_4), yellow ochre (FeOOH , clay)	
ST15		red	cinnabar/vermilion (HgS), red ochre (Fe_2O_3 , clay)	OM, FTIR-ATR, SEM-EDX
		light red	blanc fixe (BaSO_4), red ochre (Fe_2O_3 , clay)	
		white	bianco di Sangiovanni (CaCO_3)	
		yellow	chrome yellow (PbCrO_4), yellow ochre (FeOOH , clay)	
ST16		light blue	ultramarine blue ($\text{Na}_8\text{Al}_6\text{Si}_6\text{O}_{24}\text{S}_4$)	OM, FTIR-ATR, SEM-EDX
		red	cinnabar/vermilion (HgS), red ochre (Fe_2O_3 , clay)	
		light red	red ochre (Fe_2O_3 , clay)	
		yellow	chrome yellow (PbCrO_4)	

Sample	Images	Colors	Identified Pigments	Analytical Techniques
ST17		blue	ultramarine blue ($\text{Na}_8\text{Al}_6\text{Si}_6\text{O}_{24}\text{S}_4$)	OM, FTIR-ATR, SEM-EDX, PCS
		dark red	red ochre (Fe_2O_3 , clay)	
		light red	red ochre (Fe_2O_3 , clay)	
		white	bianco di Sangiovanni (CaCO_3)	
ST18		blue	ultramarine blue ($\text{Na}_8\text{Al}_6\text{Si}_6\text{O}_{24}\text{S}_4$)	OM, FTIR-ATR, XRD, SEM-EDX, PCS
		light blue	ultramarine blue ($\text{Na}_8\text{Al}_6\text{Si}_6\text{O}_{24}\text{S}_4$)	
		red	red ochre (Fe_2O_3 , clay)	
		yellow	yellow ochre (FeOOH , clay)	
ST19		blue	ultramarine blue ($\text{Na}_8\text{Al}_6\text{Si}_6\text{O}_{24}\text{S}_4$)	OM, FTIR-ATR, SEM-EDX, PCS
		light blue	azurite ($2\text{CuCO}_3 \cdot \text{Cu}(\text{OH})_2$)	
		dark ochre	yellow ochre (FeOOH , clay)	
		red	red ochre (Fe_2O_3 , clay)	
ST20		blue	ultramarine blue ($\text{Na}_8\text{Al}_6\text{Si}_6\text{O}_{24}\text{S}_4$)	OM, FTIR-ATR, SEM-EDX, PCS
		red	cinnabar/vermilion (HgS), red ochre (Fe_2O_3 , clay)	
		white	bianco di Sangiovanni (CaCO_3)	
		yellow	chrome yellow (PbCrO_4), yellow ochre (FeOOH , clay)	
ST21		light blue	ultramarine blue ($\text{Na}_8\text{Al}_6\text{Si}_6\text{O}_{24}\text{S}_4$)	OM, FTIR-ATR, SEM-EDX
		red	red ochre (Fe_2O_3 , clay)	
		white	bianco di Sangiovanni (CaCO_3)	
		yellow	yellow ochre (FeOOH , clay)	
ST22		light blue	ultramarine blue ($\text{Na}_8\text{Al}_6\text{Si}_6\text{O}_{24}\text{S}_4$)	OM, FTIR-ATR, SEM-EDX
		red	red ochre (Fe_2O_3 , clay)	
		yellow	yellow ochre (FeOOH , clay)	
ST23		red	yellow ochre (FeOOH , clay)	OM, FTIR-ATR, SEM-EDX
		yellow	red ochre (Fe_2O_3 , clay)	

Yellow and red ochre were identified based on XRD and FTIR patterns, and then confirmed by iron associated with silicon and aluminum in EDX maps.

The powders of sample ST1, which is colored in aqua green, were analyzed with XRD (**Figure 2**). A comparison with the instrument database revealed the presence of clinocllore ($\text{Mg}_3(\text{Mg}_2\text{Al})(\text{Si}_3\text{Al})\text{O}_{10}$), which is a member of the chlorite group, with a color that varies between yellowish green, olive green, blackish green and bluish green [5]. The characteristic peaks of calcite (CaCO_3), gypsum ($\text{CaSO}_4 \cdot 2\text{H}_2\text{O}$), bassanite ($\text{CaSO}_4 \cdot 0.5\text{H}_2\text{O}$), quartz (SiO_2) and barite (BaSO_4) were also observed.

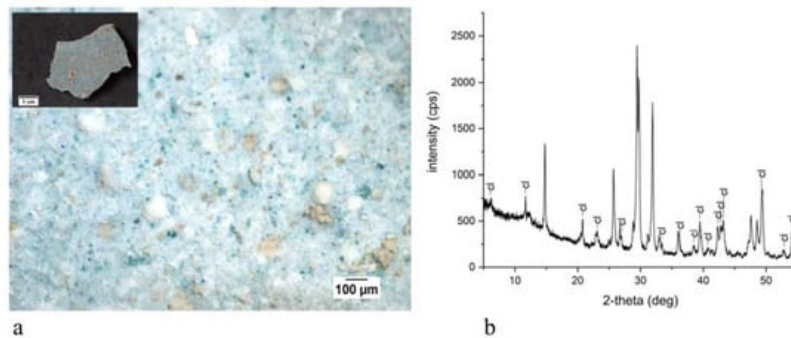


Figure 2. Aqua green area of sample ST1: digital microscope image of the surface (a) and XRD analysis on powders (b) showing the main signals of clinocllore (cl).

The pattern of IR bands (**Figure 3a**) at around 1410 cm^{-1} (C-O asymmetric stretching) and 1793 cm^{-1} (combination band), 873 and 712 cm^{-1} (C-O out-of-plane and in-plane bending vibrations, respectively) is present in all the spectra, which suggests the presence of calcium carbonate as calcite from the binder fraction of the mortar substrate [6][7][8][9][10][11]. The spectra of the white areas present only the peaks at around 1793 , 1410 , 873 and 712 cm^{-1} , which, as just discussed, refer to calcium carbonate, which constitutes the pigment bianco di Sangioanni [5].

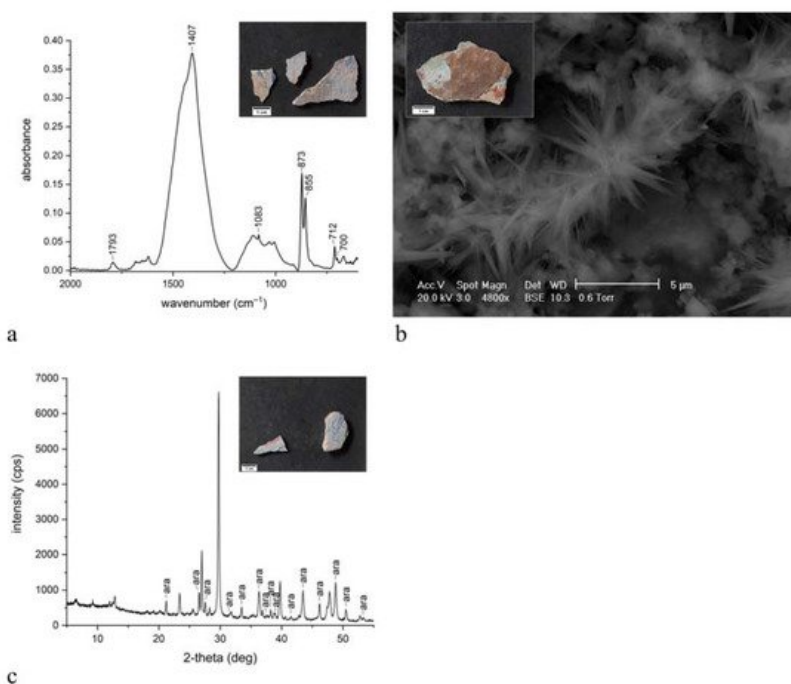


Figure 3. (a) ATR spectra of the red area of sample ST6, showing the peaks of calcite, aragonite, ochre; (b) SEM image in BSE mode of the surface of sample ST19: the typical sharp crystals of aragonite are shown; (c) XRD analysis on powders of mortar support of sample ST2, showing the main signals of aragonite (ara).

The specific peaks at around 1083 , 855 and 702 cm^{-1} found in all the samples suggest the presence of calcium carbonate in the mineralogical form of aragonite, both in the support and mixed with the pigments. The 855 and 702 cm^{-1} signals are due to ν_2 and $\nu_4\text{ CO}_3^{2-}$ vibrations, respectively, and the absorbance at 1083 cm^{-1} could be attributed to ν_1 symmetric CO_3^{2-} stretching [12][13]. **Figure 3a** shows a representative spectrum of aragonite, identified in sample ST6, where the peaks are clearly distinguished from those of calcite. SEM images of sample ST19 (**Figure 3b**) clearly showed the typical sharp, needle-like crystals of aragonite [14]. Aragonite was always corroborated by the XRD pattern, which also distinguished between the two mineralogical forms of calcium carbonate (**Figure 3c**).

In some red samples, the EDX investigations showed the distribution of mercury and sulfur in the same area, suggesting the use of cinnabar/vermillion, as in sample ST15 (**Figure 4**). Similarly, the co-presence of chrome and lead in EDX maps indicated the presence of chrome yellow, as in the yellow area in sample ST11, where the pigment was confirmed by the signals of crocoite (PbCrO_4) present in XRD results (**Figure 5**).

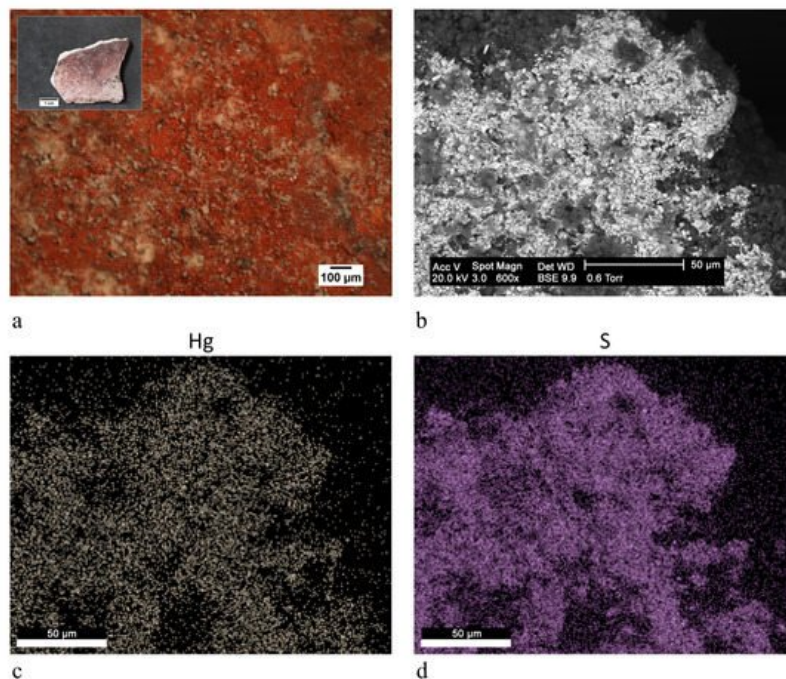


Figure 4. Red area of sample ST15: (a) digital microscope image of the surface (scale bar: 100 μm); (b) SEM image in BSE mode of the painted layer (scale bar: 50 μm); (c) EDX elemental distribution map of mercury (scale bar: 50 μm); (d) EDX elemental distribution maps of sulfur (scale bar: 50 μm).

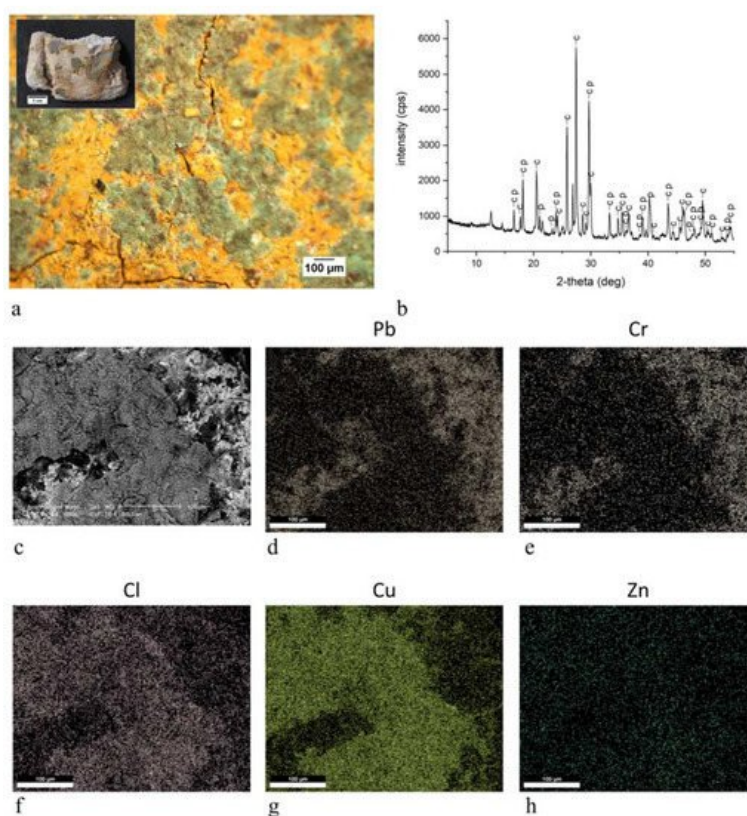


Figure 5. Yellow and green areas of sample ST11: (a) digital microscope image of the surface (scale bar: 100 μm); (b) XRD analysis on powders, showing the main signals of crocoite (c) and paratacamite (p); (c) SEM image in BSE mode of the painted layer (scale bar: 100 μm); (d) EDX elemental distribution maps of lead (scale bar: 100 μm); (e) EDX elemental distribution maps of chromium (scale bar: 100 μm); (f) EDX elemental distribution maps of chlorine (scale bar: 100 μm); (g) EDX elemental distribution maps of copper (scale bar: 100 μm); (h) EDX elemental distribution maps of zinc (scale bar: 100 μm).

The spectrum of the blue areas showed peaks at 1137, 1009 and 651 cm^{-1} , which could be attributed to Si-O-Si and Si-O-Al stretching modes of ultramarine blue ($\text{Na}_8\text{Al}_6\text{Si}_6\text{O}_{24}\text{S}_4$), respectively [45].

Blanc fixe (barium sulphate BaSO_4) was found in some samples due to the presence of IR peaks at 3606, 1089 and 659 cm^{-1} , which can be attributed to OH (surface-adsorbed water molecules), SO_4^{2-} and Ba-S-O stretching modes,

respectively [16]. EDX maps of sulfur and barium and XRD patterns of barite recorded in the same areas corroborated the hypothesis.

Gypsum was present in most samples, as highlighted by the XRD results and by the IR signals at around 3530 and 3400 (hydroxyl stretching bands), 1683 and 1621 (hydroxyl bending vibrations), 1113 (SO asymmetric stretching), and 668 cm^{-1} (SO asymmetric bending mode) [17].

Some samples presented IR patterns showing absorbances at around 1645 and 1322 (C-O stretching vibration) and 668 cm^{-1} (O-C-O bending vibrations), which were ascribed to calcium oxalate ($\text{CaC}_2\text{O}_4 \cdot n\text{H}_2\text{O}$) [17]. The spectra also show the signals at around 2918, 2850 and 1733 cm^{-1} , which suggest the CH and C=O stretching absorption of organic compounds, respectively, but were too weak and few for a reliable identification [6].

In a few green areas, zinc, chlorine and copper appeared to be associated in the EDX maps, as observed in samples ST8 and ST11 (Figure 5 and Figure 6). The combination of these elements suggests the compound $((\text{Cu,Zn})_2(\text{OH})_3\text{Cl})$, known as Brunswick green. XRD analyses of the same samples suggested the presence of the natural equivalent of the pigment, i.e., paratacamite (Figure 5). In sample ST11, Brunswick green was identified in green areas close to yellow areas painted with chrome yellow, as clearly shown in Figure 5.

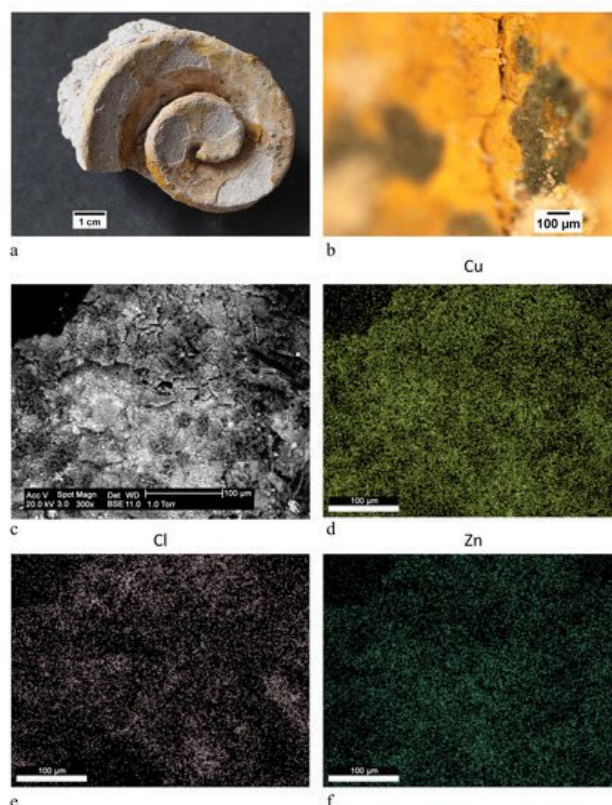


Figure 6. Green area of sample ST8: (a) image of the sample; (b) digital microscope image of details of the green areas of the painted surface (scale bar: 100 μm); (c) SEM image in BSE mode of the painted layer (scale bar: 100 μm); (d) EDX elemental distribution map of copper (scale bar: 100 μm); (e) EDX elemental distribution maps of chlorine (scale bar: 100 μm); (f) EDX elemental distribution maps of zinc (scale bar: 100 μm).

With regards to stratigraphical studies, optical and electronic microscopy revealed a number of colored layers ranging from three to eight. A combination of the EDX elemental maps recorded along the stratigraphy and the IR analysis of the single layers taken, where possible, with micro scalpel, suggested the pigments present in the samples (Table 1). Ochre is the most common pigment, generally alternated with bianco di Sangioanni white and ultramarine blue. In samples ST3 and ST13, the EDX maps recorded the signals of barium and chrome in the same areas (Figure 7). The combination of these two elements resembles the pigment barium chromate called ultramarine yellow or lemon yellow [5]. Analysis of the polished cross sections revealed strange combinations of pigments. Figure 8 shows the stratigraphy of sample ST20. The inner red layer seems to consist of the overlapping of a layer of cinnabar/vermilion and ochre, due to the presence of an accumulation of mercury and iron, respectively. On the other hand, the alternation of only ochre and azurite was observed in sample ST19.

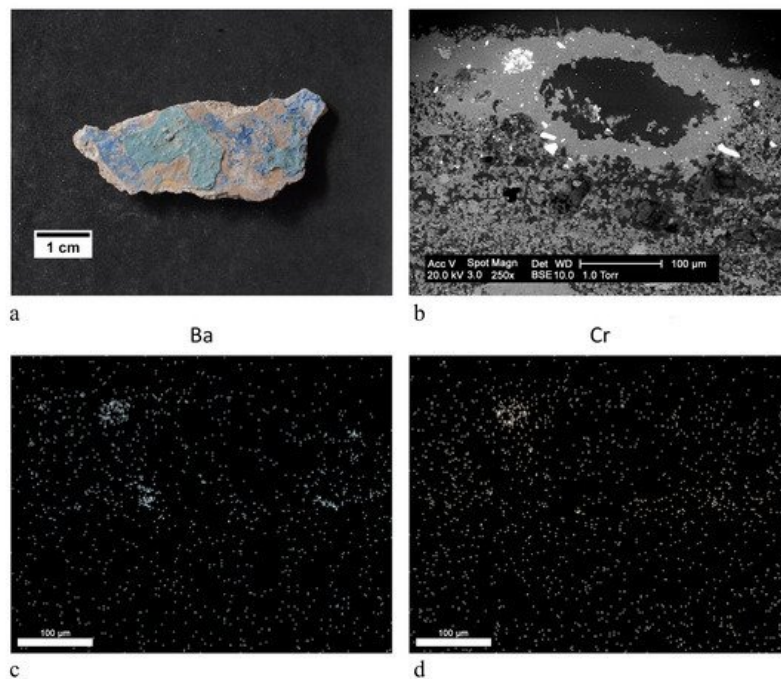


Figure 7. Yellow area of sample ST3: (a) image of the sample; (b) SEM image in BSE mode of the painted layer (scale bar: 100 µm); (c) EDX elemental distribution map of barium (scale bar: 100 µm); (d) EDX elemental distribution maps of chromium (scale bar: 100 µm).

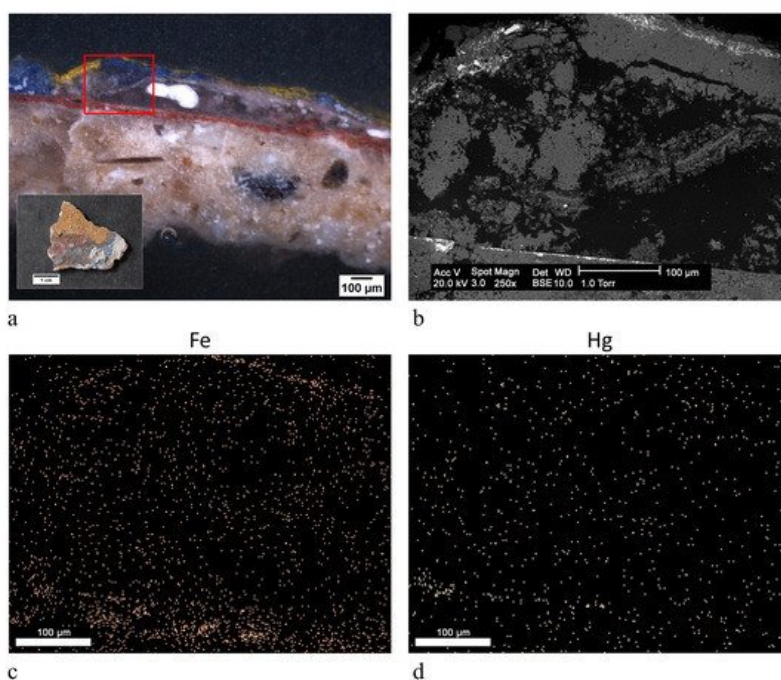


Figure 8. Polished cross section of sample ST20: (a) digital microscope image of the surface (scale bar: 100 µm); (b) SEM image in BSE mode of the painted layer (scale bar: 100 µm). The analyzed area roughly corresponds to the area evidenced in red in the figure (a); (c) EDX elemental distribution map of iron (scale bar: 100 µm); (d) EDX elemental distribution maps of mercury (scale bar: 100 µm).

3. Discussion

The analysis of the wall paintings of the church of S. Stefano attest to the use of a rich palette of colors and reveal a palimpsest of various painting cycles, as highlighted by the presence of multilayered stratigraphies. Together with common colors, such as ochre, ultramarine blue, bianco di Sangioanni, cinnabar/vermilion, azurite, a few unusual pigments were identified, specifically clinocllore, Brunswick green, ultramarine yellow, which have rarely been found in painted works of art and never in wall paintings. The presence of these pigments datable to the 19th century, indicate a terminus post quem for the execution of the external pictorial layers. Under the microscope, the underlying layers do not appear to be particularly decayed and therefore did not need to be hidden with other colors. This suggests that the building was painted regularly following whatever tastes were current at the time, using synthetic pigments available on

the market from the 19th century. Indeed, there are no records on the most recent restoration works and pictorial cycles. Thus, the identification of modern pigments contributes to shedding light on the non-documented history of the monument.

The results unfortunately also reveal, as expected, the dramatic past and present state of conservation of the paintings. Most have come away from the support; however, those that still survive have been covered on the surface by gypsum and calcium oxalate.

Finally, the ubiquitous presence of aragonite due to the intentional use of shells as an aggregate in mortar is particularly interesting. What is surprising is that the literature shows that this is the only case of this finding in wall paintings that are not from the Roman era. This therefore reveals the use of a building technology from the past in this area of the Apennines, perhaps due to its proximity to the Trebbia River and the Ligurian Sea. It is worth highlighting the importance of this area in trade between the Po Valley and Liguria. It was therefore a very frequented area, probably with the exchange of building practices that could have entailed the use of shells in mortars. It would be interesting to investigate other historical buildings in the area of Cerignale, as the discovery elsewhere of aragonite in mortars would corroborate our hypothesis. Shells were probably used as light aggregate and were therefore easy to transport to the church of S. Stefano, which is located far from the main roads and at an altitude of 700 m. The shells may have originated from the Trebbia River, in the valley below, or in the Ligurian sea, to which the Trebbia valley was connected.

The analyses carried out provide evidence of the unexpected richness and variety of the paintings in the church of S. Stefano, which is at real risk of fading. It is thus important to underline the fundamental role of conservation science, which, by studying the techniques and materials used by the artists of the past, may encourage future restoration projects and enhances and preserves the disappearing beauty.

References

1. Wilson, M.J. *Clay Mineralogy: Spectroscopic and Chemical Determinative Methods*; Chapman & Hall: London, UK, 1994; ISBN 9780412533808.
2. Bikiaris, D.; Daniilia, S.; Sotiropoulou, S.; Katsimbiri, O.; Pavlidou, E.; Moutsatsou, A.P.; Chrysoulakis, Y. Ochre-differentiation through micro-Raman and micro-FTIR spectroscopies: Application on wall paintings at Meteora and Mount Athos, Greece. *Spectrochim. Acta Part A Mol. Biomol. Spectrosc.* 2000, 56, 3–18.
3. Bugini, R.; Corti, C.; Folli, L.; Rampazzi, L. Unveiling the Use of Creta in Roman Plasters: Analysis of Clay Wall Paintings from Brixia (Italy). *Archaeometry* 2017, 59, 84–95.
4. Crupi, V.; La Russa, M.F.; Venuti, V.; Ruffolo, S.; Ricca, M.; Paladini, G.; Albin, R.; Macchia, A.; Denaro, L.; Birarda, G.; et al. A combined SR-based Raman and InfraRed investigation of pigmenting matter used in wall paintings: The San Gennaro and San Gaudioso Catacombs (Naples, Italy) case. *Eur. Phys. J. Plus* 2018, 133, 369.
5. Eastaugh, N.; Walsh, V.; Chaplin, T.; Siddall, R. *Pigment Compendium: A Dictionary and Optical Microscopy of Historical Pigments*; Pigment Compendium: A Dictionary and Optical Microscopy of Historical Pigments; Butterworth-Heinemann: Oxford, UK, 2008; ISBN 9780750689809.
6. Derrick, M.R.; Stulik, D.; Landry, J.M. *Infrared Spectroscopy in Conservation Science*; The Getty Conservation Institute: Los Angeles, CA, USA, 1999; ISBN 0892364696.
7. Bugini, R.; Corti, C.; Folli, L.; Rampazzi, L. Roman Wall Paintings: Characterisation of Plaster Coats Made of Clay Mud. *Heritage* 2021, 4, 48.
8. Montoya, C.; Lanas, J.; Arandigoyen, M.; Navarro, I.; García Casado, P.J.; Alvarez, J.I. Study of ancient dolomitic mortars of the church of Santa Maria de Zamarce in Navarra (Spain): Comparison with simulated standards. *Thermochim. Acta* 2003, 398, 107–122.
9. Igea, J.; Lapuente, P.; Martínez-Ramírez, S.; Blanco-Varela, M.T. Characterization of mudejar mortars from St. Gil Abbot church (Zaragoza, Spain): Investigation of the manufacturing technology of ancient gypsum mortars. *Mater. Constr.* 2012, 62, 515–529.
10. Biscontin, G.; Pellizon Birelli, M.; Zendri, E. Characterization of binders employed in the manufacture of Venetian historical mortars. *J. Cult. Herit.* 2002, 3, 31–37.
11. Crupi, V.; D'Amico, S.; Denaro, L.; Donato, P.; Majolino, D.; Paladini, G.; Persico, R.; Saccone, M.; Sansotta, C.; Spagnolo, G.V.; et al. Mobile Spectroscopy in Archaeometry: Some Case Study. *J. Spectrosc.* 2018, 2018, 1–11.
12. Zhang, K.; Grimoldi, A.; Rampazzi, L.; Sansonetti, A.; Corti, C. Contribution of thermal analysis in the characterization of lime-based mortars with oxblood addition. *Thermochim. Acta* 2019, 678, 178303.

13. Zhang, K.; Corti, C.; Grimoldi, A.; Rampazzi, L.; Sansonetti, A. Application of Different Fourier Transform Infrared (FT-IR) Methods in the Characterization of Lime-Based Mortars with Oxblood. *Appl. Spectrosc.* 2019, 73, 479–491.
 14. Žigovečki Gobac, Ž.; Posilović, H.; Bermanec, V. Identification of biogenetic calcite and aragonite using SEM. *Geol. Croat.* 2009, 62, 201–206.
 15. Roy, A. *Artists' Pigments: A Handbook of Their History and Characteristics*; Oxford University Press: London, UK, 1993; Volume 2, ISBN 9780894681899.
 16. Aroke, U.O.; Abdulkarim, A.; Ogubunka, R.O. Fourier-transform Infrared Characterization of Kaolin, Granite, Bentonite and Barite. *ATBU J. Environ. Technol.* 2013, 6, 42–53.
 17. Ranalli, G.; Bosch-Roig, P.; Crudele, S.; Rampazzi, L.; Corti, C.; Zanardini, E. Dry biocleaning of artwork: An innovative methodology for Cultural Heritage recovery? *Microb. Cell* 2021, 8, 91–105.
-

Retrieved from <https://encyclopedia.pub/entry/history/show/36916>